www.czasopisma.pan.pl PAN POLSKA AKADEMIA NAUK www.journals.pan.pl

Arch. Metall. Mater. **67** (2022), 2, 435-440

DOI: https://doi.org/10.24425/amm.2022.137774

A. DZIADOŃ[1*], E. MUSIAŁ[1]

EFFECTS OF POST-WELD HEAT TREATMENT ON THE MICROSTRUCTURE AND MECANICAL PROPERTIES OF THE AZ91 LASER WELDED JOINT

Plates of AZ91 magnesium alloy were butt-welded using a CO_2 laser. The non-equilibrium solidification of the laser-melted metal caused fragmentation of the weld microstructure as well as the supersaturation of a solid solution of aluminium in magnesium, which enabled the T5 ageing of the weld. The weld proved to be a mechanically stable part of the joint; all the tensile-tested specimens, both as-welded and post-weld T5 aged, fractured outside it. During the ageing of the supersaturated joint, which involved heat treating it to the T6 condition, the weld was the region where discontinuous precipitation was observed and this was the location of fracture in the tensile specimens. Thus, the strength properties of welded, supersaturated and aged AZ91 were much worse than when the non-welded material was T6 tempered.

Keywords: AZ91 alloy; laser welding; heat treatment after welding

1. Introduction

Magnesium alloys are attractive materials used increasingly in a wide range of structural and mechanical applications mainly because of their low density. They are commonly used, e.g. in the electronics, automotive and aerospace industries. Nearly 90% of magnesium alloy details are manufactured by casting [1,2]. Mg-Al-Zn casting alloys are widely used both because of their favourable properties and relatively low prices [3]. An example is AZ91, which combines excellent castability with good mechanical properties at temperatures not exceeding 100°C and acceptable corrosion resistance [1,4-7].

The literature on the subject includes a number of papers on AZ91 alloy welding using either GTAW [8-11] or the laser method [12-16]. Few, however, have dealt with the heat treatment of welded magnesium alloys, despite the fact that most of these materials, including AZ91, can be precipitation strengthened. The influence of post-weld heat treatment on the microstructure and mechanical properties of magnesium alloys has been described for AZ31 [17-19], AZ90 [20] A80 [21] as well as for magnesium alloys with rare earth metals [22-24]. The studies on AZ31 and A80 described the effects of annealing; the investigation on AZ90 focused on aging after friction stir processing; and only the research on magnesium alloys with rare earth metals dealt with precipitation strengthening (T6 treatment).

In supersaturated and aged Mg-Al alloys, discontinuous precipitation involves the growth of the lamellar structure made up of alternating layers of $Mg_{17}Al_{12}$ and the near-equilibrium magnesium matrix phase (a solid solution of aluminium in magnesium). Continuous precipitation occurs due to the nucleation and growth of individual particles of the $Mg_{17}Al_{12}$ phase dispersed in the magnesium matrix. These two types of precipitation take place in the supersaturated AZ91 alloy competitively and simultaneously [25-28].

This study aimed to analyse the structural processes taking place during post-weld ageing and their effects on the strength of welded AZ91 alloy.Two types of heat treatment were considered: T5 and T6, with the former involving ageing immediately after welding and the latter consisting of supersaturation and ageing.

2. Experimental procedure

The investigations were carried out for commercial AZ91 magnesium alloy (9.11 wt.% Al, 0.64 wt.% Zn and 0.23 wt.% Mn). The specimens were prepared from an ingot cut perpendicular to its longitudinal axis. The ingot was approximately 550 mm long and 50 mm high; it was trapezoidal in cross-section (100 × 120 mm). It was machined to the dimensions of the cross-section 100 × 50 mm. The specimens were in the form of

[1] KIELCE UNIVERSITY OF TECHNOLOGY, METALS SCIENCE AND MATERIALS TECHNOLOGIES, 7 TYSIĄCLECIA PAŃSTWA POLSKIEGO AV., 25-314, KIELCE, POLAND

* Corresponding author: adziadon@tu.kielce.pl

plates with a thickness of 3.5 mm, a length of about 100 mm, and a width of about 50 mm. The plates were then cut across, along a dimension of 50 mm into two halves, which were mechanically clamped into position to be butt-welded along the cut line. A TRUMPF TLP 6000 CO_2 laser system was used for the welding. The shielding gas was helium (10 l/min). The laser beam had a diameter of 0.3 mm. The welding process involved applying a laser power of 2000 W and a welding speed of 4 m/min. The choice of the parameters was based on the authors' previous findings [29]. In this study, the major optimisation criterion was the minimisation of the weld porosity. When welding is performed at a speed of 4 m/min, no macroporosity is observed and also the weld width and face concavity are reduced [29].

The heat treatment parameters used in this study for AZ91 were those proposed by Avedesian and Baker in [30]. The T5 temper was achieved by holding the material for 16 hours at a temperature of 170°C. The heat treatment to the T6 condition required holding the specimens for 24 hours at 420°C, quenching them in water and, finally, ageing them for 16 hours at a temperature of 170°C.

The specimens were tested in five groups: as-cast (non-welded), welded, welded and T5 aged, welded and T6 tempered, and non-welded (as-cast) and T6 tempered. The microstructure variations and the Vickers hardness distributions were studied in the cross-sections perpendicular to the welding direction. The Vickers hardness measurements were carried out at a load of 10 kg. Optical and scanning electron microscopy required using standard metallographic methods of specimen preparation. The optical microscopy (OM) observations were conducted by means of a NIKON ECLIPSE MA200 and a METAVAL, to obtain greater and lower magnification images, respectively. The scanning electron microscopic (SEM) analysis involved employing a JEOL JSM-5400 equipped with an OXFORD INSTRUMENTS ISIS 300 energy dispersive X-ray analysis system. Tensile testing was performed at an initial strain rate of 4.7×10^{-4} sec^{-1} using a LAB Test 5.20 SP1 screw-driven machine. Figure 1 shows the dimensions of a tensile specimen with the weld located in the centre of the gauge length. The specimens prepared from non-welded materials were of the same geometry. A total of five specimens were tensile tested to failure for each case considered.

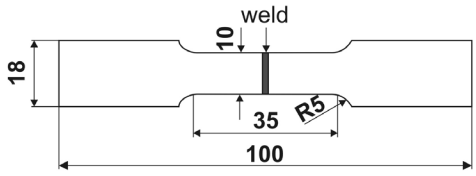

Fig. 1. Geometry of the tensile specimen

3. Results

3.1. Microstructure of the base material

The predominant phase of the microstructure of the as-cast AZ91 alloy (Fig. 2) is a solid solution of aluminium in magnesium (α-phase), which solidifies in the form of dendrites at the beginning of the crystallisation process. In accordance with the phase equilibrium system, the Mg-Al [31] eutectic, which solidifies between the dendrites, consists of the intermetallic $Mg_{17}Al_{12}$ phase and the α-phase. Discontinuous precipitates are also observed, and that is the result of partial decomposition of the solid solution of aluminium in magnesium. They are the dark areas in the microstructure image (Fig. 2).

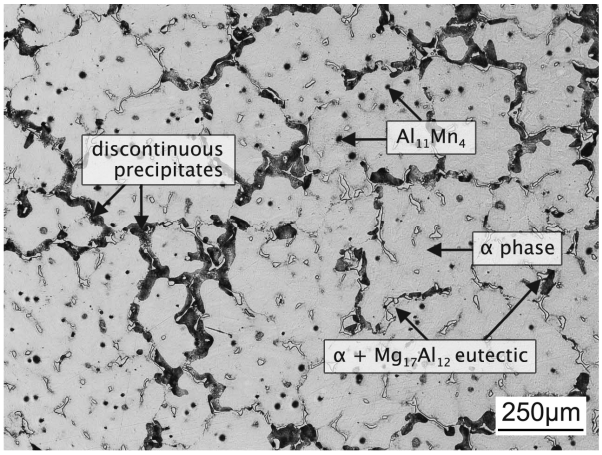

Fig. 2. OM microstructure of the as-cast AZ91 alloy

As determined by the EDS analysis, the phase defined as $Mg_{17}Al_{12}$ has the following composition: 61.8 at.% Mg, 36.4 at.% Al and 1.8 at.% Zn. The dendrites contain 5-7% Al and 0.2% Zn. According to the EDS analysis, the dark, equiaxed particles distributed in the dendrites (Fig. 2) are particles of the $Al_{11}Mn_4$ phase.

3.2. Microstructure of the welded joint

Figure 3a shows the joint microstructure observed in the cross-section. The very fast transfer of heat from the fusion zone (FZ), where the material was liquid, to the cool surrounding

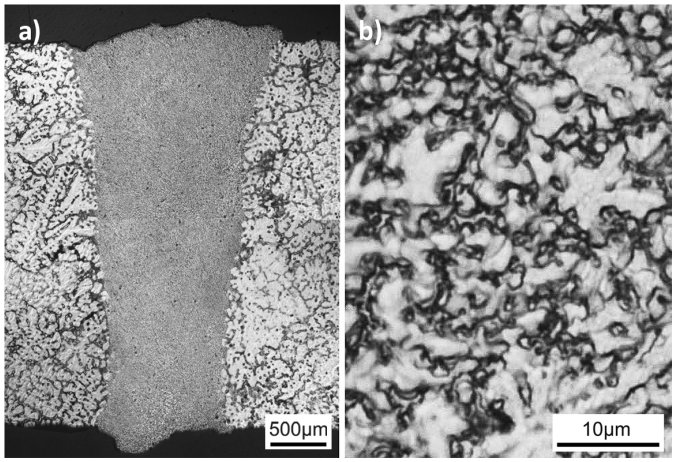

Fig. 3. Microstructure of the welded joint (a) and higher OM magnification image of the weld microstructure (b)

base metal caused rapid solidification and considerable dispersion of the weld microstructure constituents, in particular the $Mg_{17}Al_{12}$ particles. The microstructure of the weld consists of fine dendrites (α-phase) and a eutectic with very small $Mg_{17}Al_{12}$ particles (Fig. 3b, the higher magnification image).

3.3. Effects of the heat treatment on the microstructure and mechanical properties of the welded joint

The hardness distribution plots and the SEM images of the weld microstructure are provided in Fig. 4. Hardness was measured in the specimen cross-section in the weld and the adjacent areas. In the as-welded condition, the hardness of the weld was higher than that of the base material (Fig. 4a). The T5 ageing caused a further increase in the weld hardness (Fig. 4b); there was also a slight increase in the hardness of the base material. After the T6 temper, the hardness of the weld was similar to that outside it (Fig. 4c); still, it was lower than the value reported for the weld, which had not undergone heat treatment. The SEM image in Fig. 4a shows the microstructure of the weld for a welded joint not subjected to heat treatment.

As can be seen, it is the eutectic: the $Mg_{17}Al_{12}$ phase and the α-phase (a solid solution of aluminium in magnesium). The T5 ageing resulted in the formation of precipitates in the weld zone, which were mainly discontinuous. From Fig. 4b, it is evident that they are located around particles of the eutectic $Mg_{17}Al_{12}$ phase. The heat treatment to the T6 condition (Fig. 4c) caused discontinuous precipitation at the grain boundaries of the α-phase matrix and continuous precipitation inside the grains.

TABLE 1 shows the average values of the yield strength, tensile strength and elongation obtained for the specimens with welded joints before and after heat treatment. The tensile properties were also determined for the as-cast AZ91 alloy and the as-cast AZ91 alloy subjected to precipitation strengthening (T6 temper). The information provided in TABLE 1 includes the location of fracture for all the specimen types.

The strength properties of the welded joints heat-treated to the T6 condition were much lower than those of the non-welded T6 heat treated specimens. All the welded specimens heat-treated

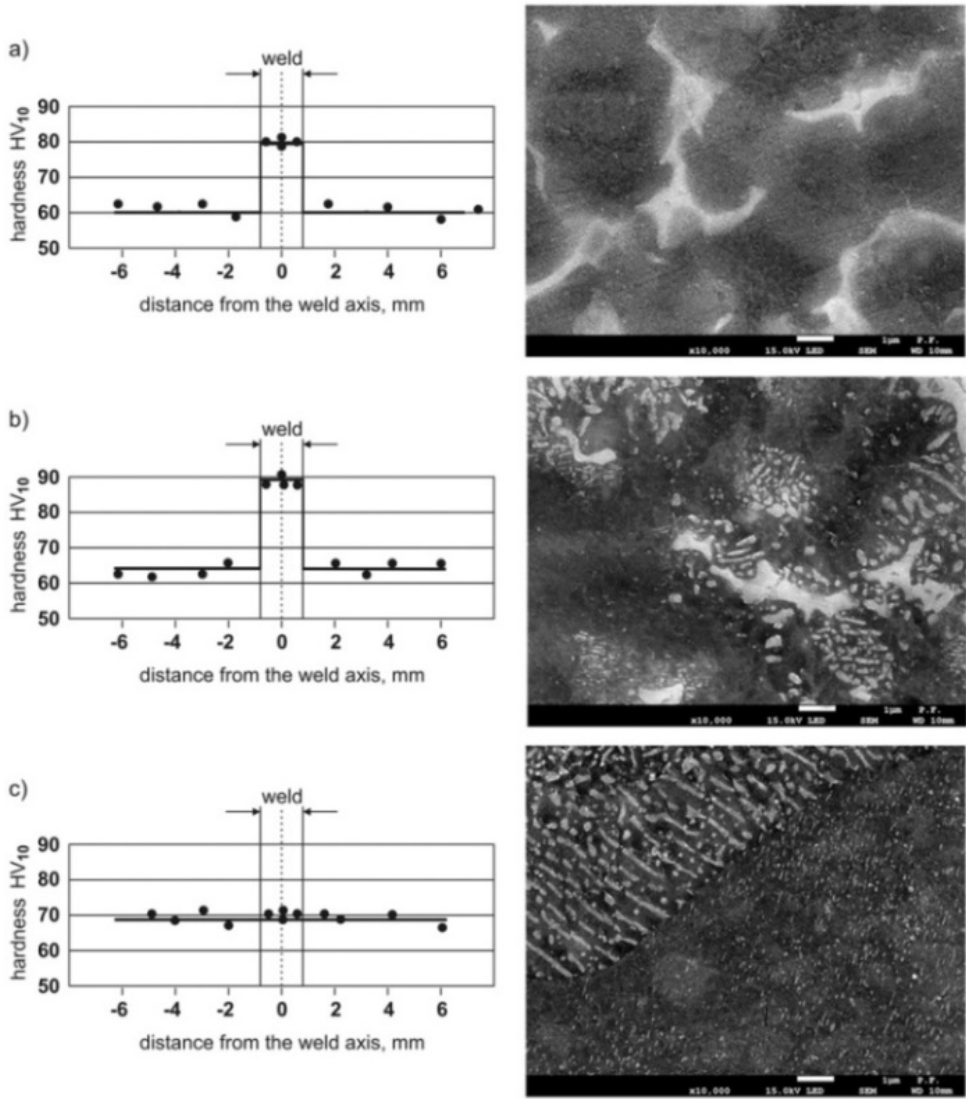

Fig. 4. Hardness distribution plots and the SEM images of the weld microstructure for: (a) welded, (b) welded and T5 aged, (c) welded and T6 tempered AZ91 specimens

TABLE 1

Tensile properties of the AZ91 specimens

AZ91 alloy	Yield strength $R_{0.2}$, MPa	Tensile strength R_m, MPa	Elongation A, %	Fracture location
As-cast	65	120	3.0	base material
Welded	71	119	2.0	base material
Welded, T5 aged	77	137	2.0	base material
Welded, T6 tempered	82	149	2.8	fusion zone
As-cast, T6 tempered	121	196	6.8	base material

to the T6 condition fractured in the weld during tensile testing, while in all the other cases, the fracture was located outside the weld, in the base material.

After the tensile test, the fracture surface of the welded and T6 heat-treated specimens was examined microscopically. An example is shown in Fig. 5. The microstructural analysis was carried out in several sections of the specimen running transversely through the cracked weld. Figure 5a shows the material microstructure across half the length of the weld – from one edge to the axis of the tensile specimen. Figures 5b and 5c illustrate the weld microstructures in the cross-sections on the other (opposite) side of the axis of the tensile specimens, which are located at different distances from the axis. The higher magnification images in Figs. 5d and 5e reveal that the microstructural elements observed in the weld are colonies of discontinuous precipitation. The distribution of discontinuous precipitates is not homogeneous; it should be noted, however, that they were always observed in the region between the fusion zone and the

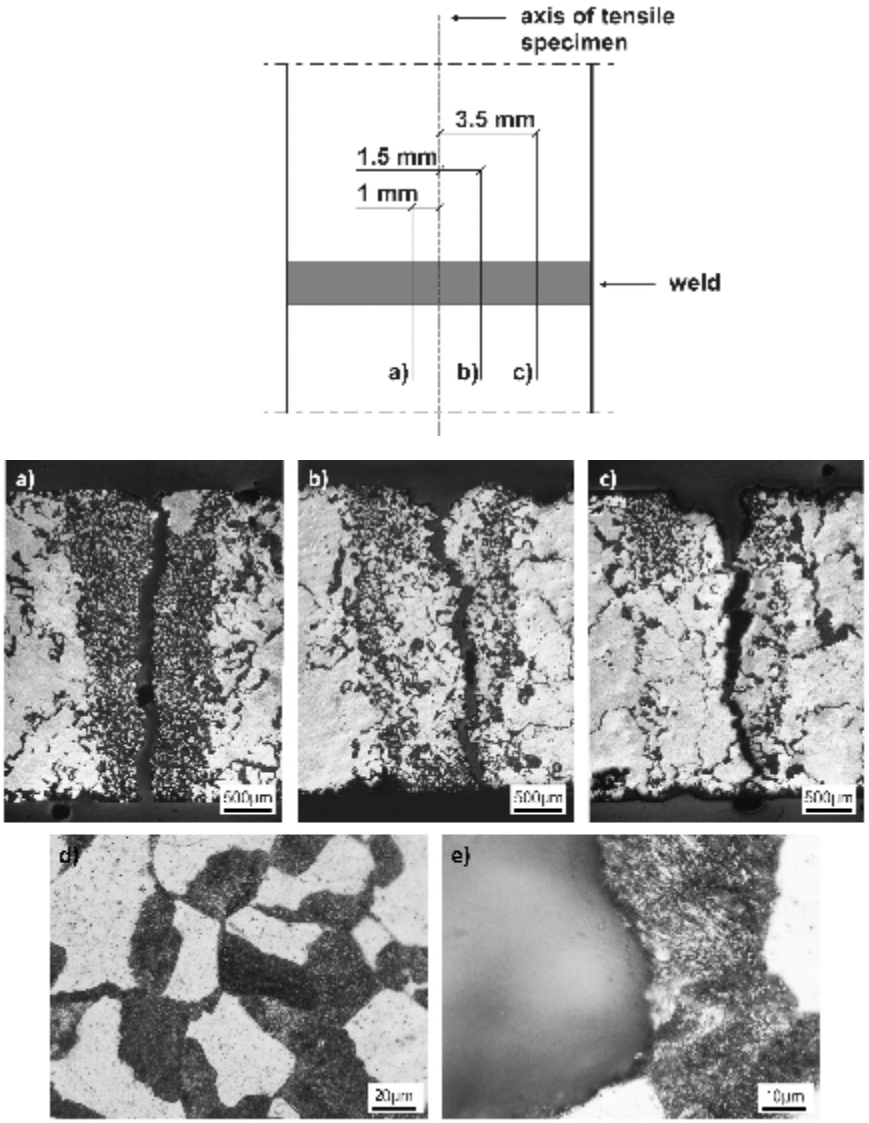

Fig. 5. OM microstructures of the welded T6 tempered specimens after tensile testing: (a) microstructure of the weld between one edge of the tensile specimen and its axis of symmetry; (b) (c) microstructures of the weld on the other side of the axis at distances of 1.5 mm and 3.5 mm from the axis, respectively; (d, e) higher magnification OM images of the weld microstructure with clearly visible discontinuous precipitates in the area adjacent to the fracture and in the fracture area, respectively

base material. The examination of the tensile fracture surface of the T6 tempered AZ91 specimens revealed that the fracture in the areas of discontinuous precipitation is of the brittle type. Figure 6 shows SEM images of the cleavage fracture of the layered structure formed from the lamellae of the $Mg_{17}Al_{12}$ and the α phases. It seems that the cracking was initiated at the $Mg_{17}Al_{12}$/α-phase interface.

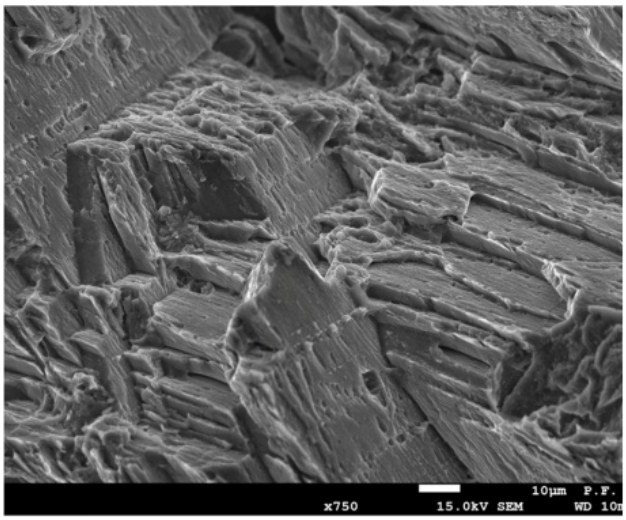

Fig. 6. SEM images of the fracture surfaces of the AZ91 tensile specimen showing fractographic features of the lamellar region

To explain the cause of the extensive discontinuous precipitation taking place in the weld, it was necessary to analyse the changes in the weld microstructure during heat treatment to the T6 condition. The examination of the microstructure after supersaturation (Fig. 7a) shows grains of the solid solution of aluminium (and zinc) in magnesium and particles of the intermetallic aluminium-manganese $Al_{11}Mn_4$ phase, with the latter not affected by the heat treatment process. A characteristic feature of the weld microstructure is the non-uniformity of the grain size. In the section of the weld shown in Fig. 7a, there are groups of fine grains, located mainly along the weld line. During ageing, the number of discontinuous precipitates is much higher in the areas of the fine-grained structure (Fig. 7b). Thus, the reason for the intense discontinuous precipitation process in some areas of the weld is the grain refinement in the supersaturated state.

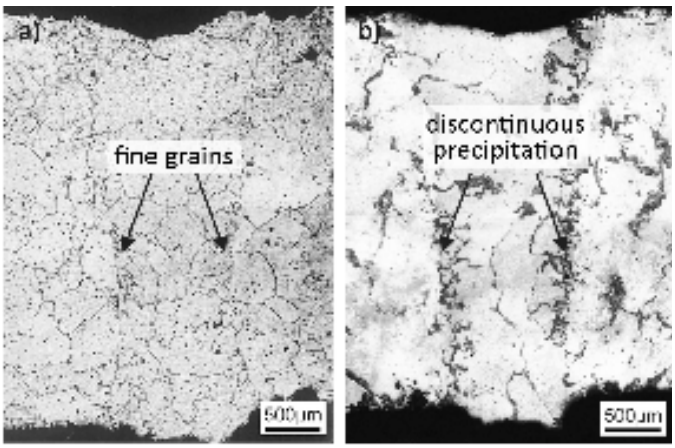

Fig. 7. OM images of the weld microstructure after (a) supersaturation, (b) ageing

4. Discussion

The rapid loss of heat between the fusion zone and the base metal leads to the refinement of the weld microstructure. As a result of a high degree of dispersion of the $Mg_{17}Al_{12}$ particles, the FZ becomes the hardest part of the joint. Another effect of the non-equilibrium solidification of the alloy melted by the laser beam was the supersaturation of the solid solution of aluminium in magnesium. The degree of supersaturation was large enough to improve the weld hardness during ageing (heat treatment to the T5 condition). The weld was reported to be a mechanically stable part of the welded joint both before and after the heat treatment to the T5 condition; the tensile test results show that the welded as well as the welded and T5 aged specimens fractured in the base material.

The heat treatment to the T6 condition following welding increased the hardness of the base material but reduced the hardness of the weld. The hardness measured in the fusion zone did not differ much from the hardness of the base material; it was lower than the hardness of the weld in a non-heat treated joint. It is clear that the fine eutectic that formed during the welding caused greater strengthening of the weld than the conventional T6 heat treatment. It is important to note that heat treatment to the T6 condition performed after welding made the weld the weakest part of the joint. All the welded T6 tempered specimens subjected to tensile testing fractured in the weld. From the microstructural examination, it appears that this was due to discontinuous precipitation in some areas of the fusion zone, which formed during the ageing of the supersaturated joint. Discontinuous precipitation is reported to occur extensively in fine-grained areas of the weld. A high dispersion of the weld microstructure is likely to be responsible for a larger number of α-phase nuclei formed during heating in the fusion zone than outside it. Part of them do not grow into coarse grains under standard heat treatment conditions (holding at 420°C for 24 hours) and, like fine grains, remain unchanged in the weld structure after supersaturation.

Nucleation of discontinuous precipitation at high-angle grain boundaries is well documented both for AZ91 [26-28] and for other alloys [32,33]. In fine-grained welds, the total high-angle grain boundary area is larger than that in the coarse-grained structure; thus, there are more potential sites for nucleation of discontinuous precipitates. The morphology of the discontinuous precipitates (colonies of lamellae containing the $Mg_{17}Al_{12}$ plate-shaped phase, which is brittle [34,35]) promotes cleavage fracture of this structure.

Due to the fragile weld, the welded joint did not reach the desirable tensile properties, similar to those observed for unwelded, T6 tempered AZ91. After the heat treatment to the T6 condition, the yield strength and tensile strength of the welded joint increased only by 17 MPa ($R_{0.2}$ = 82 MPa) and 29 MPa

(R_m = 149 MPa), respectively, when compared with the values reported for the as-cast alloy. The increase in the strength properties was moderate because of the fracture in the fusion zone. By contrast, the unwelded, T6 tempered AZ91 alloy had $R_{0.2}$ = 121 MPa and R_m = 196 MPa.

Finally, it should be noted that as reported in the literature, precipitation strengthening of laser-welded joints of magnesium alloys with rare earth metals does not weaken the weld. The ageing of these alloys was found to occur without discontinuous precipitation. As a result, the tensile strength of the joints of the Mg-Nd-Zn-Zr [22] or Mg-Gd-Y-Zr [23,24] alloys can be improved significantly when the welded joint is heat treated to the T6 condition.

5. Conclusions

1. The weld produced by the laser welding of AZ91 alloy had a fine eutectic microstructure. The hardness of the weld was about 30% greater than that of the base material. It is possible to further increase the hardness of the weld by subjecting it to ageing (heat treatment to the T5 condition).
2. The tensile test results show that the weld is able to withstand a greater load than the base material; all the welded specimens, whether heat-treated to the T5 condition or not, fractured outside the weld zone.
3. The T6 temper of welded AZ91 leads to the formation of a large number of non-uniformly distributed discontinuous precipitates in the weld.
4. The examination of the tensile fracture surface of the T6 tempered AZ91 specimens revealed that the fracture in the areas of discontinuous precipitation was of the brittle type.
5. The tensile data indicate that, mechanically, the weld was the weakest part of the T6 heat-treated joint; all the tensile specimens fractured in the weld.

REFERENCES

[1] R.L. Edgar, Global overview on demand and application for magnesium alloys, in: K.U. Kainer (Ed.), Proceedings of the International Conference on Magnesium Alloys and Their Applications, Wiley-Vch. (2000).
[2] F. Pan, M. Yang, X. Chen, J. Mater. Sci. Technol. **32**, 1211-1221 (2016).
[3] A. Luo, M.O. Pekguleryus, J. Mater. Sci. **29**, 5259-5271 (1994).
[4] I.J. Polmear, Mater. Sci. Tech. **10**, 1-16 (1994).
[5] C.H. Cáceres, D.M. Rovera, J. Light Metals. **1**,151-156 (2001).
[6] M. Regev, E. Aghion, A. Rosen, R. Bamberger, Mater. Sci. Eng. A. **252**, 6-16 (1998).
[7] G. Song, A.L. Bowles, D.H. StJohn, Mater. Sci. Eng. A. **366**, 74-86 (2004).
[8] A. Munitz, C. Cotler, A. Stern, G. Kohn, Mater. Sci. Eng. A. **302**, 68-73 (2001).
[9] T. Zhu, Z. W. Chen, W. Gao, Mater. Sci. Eng. A. **416**, 246-252 (2006).
[10] J. Shen, G. You, S. Long, F. Pan, Mater. Charact. **59**, 1059-1065 (2008).
[11] K.N. Braszczyńska-Malik, M. Mróz, J. Alloys Compd. **509**, 9951-9958 (2011).
[12] M. Marya, G.R. Edwards, J. Mater. Eng. Perform. **10**, 435-443 (2001).
[13] M. Dhahri, J.E. Masse, J.F. Mathieu, G. Barreau, M. Autric, Adv. Eng. Mater. **3**, 504-507 (2001).
[14] X. Cao, M. Jahazi, J.P. Immarigeon, W. Wallace, J. Mater. Proc. Technol. **171**, 188-204 (2006).
[15] K. Abderrazak, W.B. Salem, H. Mhiri, P. Bournot, M. Autric, Metall. Mater. Trans. B. **40**, 54-61 (2009).
[16] M. Wahba, M. Mizutani, Y. Kawahito, S. Katayama, Mater. Design. **33**, 569-576 (2012).
[17] Z. Yan, H. Zhang, J. Duan, F. Liu, G. Wang, J. Wuhan University of Technology-Mater. Sci. Ed. **32**, 1205-1212 (2017).
[18] S. Fukumoto, D. Yamamoto, T. Tomita, K. Okita, H. Tsubakino, A. Yamamoto, Mater. Trans. **48**, 44-52 (2007).
[19] X. Wang, J. Zhang, Chem. Eng. Trans. **66**, 367-372 (2018).
[20] A.H. Feng, Z.Y. Ma, Acta Mater. **57**, 4248-4260 (2009).
[21] T.C. Tsai, C.C. Chou, D.M. Tsai, K.T. Chiang, Mater Design. **32**, 4187-4194 (2011).
[22] J. Dai, J. Huang, M. Li, Z. Li, J. Dong, Y. Wu, Mater. Sci. Eng. A. **529**, 401-405 (2011).
[23] L. Wang, J. Huang, J. Dong, K. Feng, Y. Wu, P.K. Chu, Mater. Charact. **118**, 486-493 (2016).
[24] L. Wang, J. Huang, J. Dong, Z. Li, Y. Wu, Weld World. **61**, 299-306 (2017).
[25] D. Duly, J.P. Simon, Y. Brechet, Acta Metall. Mater. **43**, 101-106 (1995).
[26] S. Celotto, T.J. Bastow, Acta Mater. **49**, 41-51 (2001).
[27] M.X. Zhang, P.M. Kelly, Scripta Mater. **48**, 647-652 (2003).
[28] K.N. Braszczyńska-Malik, J. Alloys Compd. **477**, 870-876 (2009).
[29] A. Dziadoń, E. Musiał, Arch. Foundry Eng. **20** (3) 9-14 (2020).
[30] M.M. Avedesian, H. Baker, Heat treating, in: M.M. Avedesian, H. Baker, Magnesium and Magnesium Alloys. ASM International (1999).
[31] Landolt-Börstein, Numerical data and functional relationships in science and technology, New series, Group IV: Physical chemistry, Phase equilibria, Crystallographic and thermodynamic data of binary alloys. Berlin, Springer-Verlag (1998).
[32] N.C. Santhi Srinivas, V.V. Kutumbarao, Scripta Mater. **37**, 285-291 (1997).
[33] A. Dziadoń, J. Maurer, Arch. Metall. **43**,363-374 (1998).
[34] J. Ragani, P. Donnadieu, C. Tassin, J.J. Blandin, Scripta Mater. **65**, 253-256 (2011).
[35] H.N. Mathur, V. Maier-Kiener, S. Korte-Kerzel, Acta Mater. **113**, 221-229 (2016).